PHYSICAL REVIEW A VOLUME 49, NUMBER 4 APRIL 1994

Periodic-orbit spectroscopy of the hydrogen atom in parallel electric and magnetic fields

M. A. Iken
School of Physics, Georgia Institute of Technology, Atlanta, Georgia 30332-0430

F. Borondo
Departamento de Quimica, C-XIV, Universidad Autonoma de Madrid, Cantoblanco, 28049 Madrid, Spain

R. M. Benito
Departamento de Fisica Aplicada, Escuela Técnica Superior de Ingenieros de Telecomunicacion, Universidad Politecnica de Madrid, 28040 Madrid, Spain

T. Uzer
School of Physics, Georgia Institute of Technology, Atlanta, Georgia 30332-0430
(Received 28 October 1992)

Using well-known concepts from semiclassical dynamics, we simulate spectra of a hydrogen Rydberg electron under the influence of parallel electric and magnetic fields. The spectra show peaks characteristic of recurring orbits as well as periodic orbits, which we have identified. The results agree qualitatively with experiments.

PACS number(s): 32.80.Rm, 03.65.Sq, 31.10.+z, 32.60.+i

I. INTRODUCTION

In the past decade the attention of many atomic physicists and nonlinear dynamicists has been focused on electron dynamics and spectroscopy in highly excited Rydberg atoms placed in external fields [1]. This intense interest stems from two principal reasons: These atoms can be prepared and manipulated in the laboratory [2] and they are amenable to theoretical treatments, often with astonishing accuracy [3,4]. The corresponding Hamiltonians possess seemingly simple nonlinearities which can lead to chaotic classical dynamics. The very high excitations involved imply that the detailed quantum-mechanical treatment can be very tedious; on the other hand, the same excitations usually place the electron into a regime where reasonable accuracy can be expected of the correspondence principle. Thus Rydberg atoms in external fields constitute atomic laboratories in which the quantum mechanics of classically chaotic systems can be investigated [5,6].

The quadratic Zeeman effect (QZE) [3–7] is among the most often investigated atomic scenarios: Here the external magnetic field is strong enough to contribute a significant diamagnetic term to the atomic Hamiltonian (in contrast, the Stark effect in Rydberg atoms has not received the same intense attention because its Hamiltonian is separable and does not develop chaos). When the effect of the external field becomes comparable with the Coulomb field the QZE Hamiltonian leads to chaotic behavior. In the same regime, the excitation spectrum has been observed to show sinusoidal modulation of the spectral intensity [7], and unraveling these oscillations by relating advanced quantum-mechanical ideas such as the Gutzwiller level density formula [8] to the periodic orbits of the corresponding classical system have yielded valuable insights into the quantum mechanics of classically chaotic systems. Briefly, it turns out that the excitation cross section can be approximated classically as a "phasor sum" over recurring classical orbits, which include among them periodic orbits of the system. This result is intuitively reasonable once the photoabsorption spectrum is expressed as the Fourier transform of the autocorrelation function [9–13]. Its oscillations are determined by the overlap of an initial distribution with itself at different times. Indeed, this approach to the origin of quasi-Landau modulation has been illustrated beautifully by Reinhardt [11,12] using wave-packet propagation. Currently, theoretical and experimental interest in electronic wave packets is continuing [13,14].

One of the great advantages of QZE Hamiltonians is that they scale with magnetic field strength [3,4]. By suitably tying all relevant quantities to the magnetic field (i.e., by using classical magnetic units [15]), one can ensure that periodic orbits need not be reanalyzed every time the field is changed. Indeed, when working with the scaled Hamiltonian, the total energy becomes the only adjustable parameter in the analysis. It has now become desirable, however, to find other paradigmatic and experimentally realizable systems which have all the desirable properties of the QZE, but contain additional simple perturbations. One such system can be produced by adding an electric field to the strong magnetic field. Increasingly, the resulting Stark–quadratic Zeeman effect (SQZE) is attracting the interest of theorists [1,16–18] and experimentalists [19–22]. Among possible relative orientation of the fields, the parallel alignment alone ensures the survival of the magnetic quantum number as a good quantum number throughout the chaotic regime and therefore reduces the phase space of the problem to manageable size (namely, the same as the QZE). Various aspects of parallel-field SQZE, including supersymmetry [23] and the use of extended Lissajous action-angle variables for high-order perturbation theory [24], have been investigated in the recent literature.

As argued before, the presence of experimentally adjustable parameters in the parallel-field SQZE opens up the possibility of researching the evolution of the well-known QZE properties under the influence of a perturbation. Precisely such an experiment was performed by König *et al.* [20], who, with the help of high-resolution laser spectroscopy, studied the oscillator strength distribution of barium in the vicinity of the zero-field threshold [25]. In their spectra, they observed a transition from quasi-Landau resonances to electric-field-induced oscillations [26] as they increased the strength of the electric field and were able to relate many spectral features of the intermediate cases to the periodic orbits of the evolving system. These experiments constitute seminal probes into the structure of the SQZE phase space in general and the evolution and bifurcations of various periodic orbits in particular. On the other hand, they are rather difficult to simulate in detail because of the nonhydrogenic nature of barium, as well as the high excitations and extensive initial state mixing, to name just a few of the difficulties.

Our purpose in this article is to map the evolution of the hydrogen Rydberg spectrum as it changes from the magnetic-field-dominated to the electric-field-dominated regime. Because of the many technical difficulties involved in simulating the experiment, we will perform the analysis only semiquantitatively and after a number of approximations. For our investigation, we use a method which has successfully uncovered the order under the spectra of a number of classically chaotic atomic and molecular systems, namely, classical autocorrelation functions [9,10,27–31,39]. The initial excitation is assumed to be in the form of a wave packet [9,10,27] and its evolution is followed by means of quasiclassical trajectories [27]. While these classical constructs obviously do not have all feature of quantal evolution, they are known to give useful results in the correspondence principle regime. We simulate spectra by calculation of a classical low-resolution autocorrelation function [9,10,27,32,33], which shows very clearly which recurring trajectories and/or periodic orbits should be expected to contribute to the spectrum as the system evolves. This procedure is particularly well suited for identifying new periodic orbits, especially in systems with nontrivial symmetries. While experimental and calculated spectra differ in their details, there is remarkable qualitative agreement given the highly approximate nature of our treatment.

This article is organized as follows. First, the scaled Hamiltonian for the parallel-field SQZE is derived. Then we discuss the details of constructing an initial wave packet and calculating the autocorrelation function. For each electric field (including the QZE), we examine significant spectral features and trace their origins to recurring motions in the system. We find that the appearance of the spectra changes drastically for a number of critical electric-field strengths. We conclude with a discussion of possible extensions.

II. HAMILTONIAN

Here we construct the scaled Hamiltonian for a hydrogen atom in a high Rydberg state in the presence of parallel electric and magnetic fields along the lines of the work of Edmonds and Pullen [15]. A few well-founded assumptions simplify the Hamiltonian greatly. We assume that the magnetic field is large enough to cause a level splitting which is much greater than the spin-orbit splitting; thus we can ignore the spin of the electron. We also specialize our treatment to the $m=0$ state without loss of generality (the extension to nonzero m is straightforward [24]).

With the assumptions mentioned above, the Hamiltonian consists of the kinetic energy, magnetic field B, electric field F, and the Coulombic term. The Hamiltonian is first converted to a rotating Larmor frame whose frequency is half the cyclotron frequency, which is

$$\omega_c=\frac{|e|B}{\mu c} , \tag{1}$$

where μ is the reduced mass of the electron and e is the electronic charge. In cylindrical coordinates, the resulting Hamiltonian is

$$H=\frac{p_\rho^2}{2\mu}+\frac{p_\phi^2}{2\mu\rho^2}+\frac{p_z^2}{2\mu}+\frac{\omega_c^2\mu\rho^2}{8}-eFz-\frac{e^2}{(\rho^2+z^2)^{1/2}} . \tag{2}$$

Using classical magnetic units [15]

$$\mu=(\text{electron reduced mass}) , \tag{3}$$

$$\rho_0=2\left[\frac{\mu c^2}{B^2}\right]^{1/3} , \tag{4}$$

$$T=\frac{2}{\omega_c} , \tag{5}$$

$$\mathcal{E}=\frac{2e^2}{\rho_0} , \tag{6}$$

for mass, length, time, and energy, respectively, the Hamiltonian is considerably simplified to

$$H=\frac{p_\rho^2}{2}+\frac{p_\phi^2}{2\rho^2}+\frac{p_z^2}{2}+\frac{\rho^2}{2}-\frac{1/2}{(\rho^2+z^2)^{1/2}}+\frac{\lambda z}{8} , \tag{7}$$

where

$$\lambda=-\frac{16}{e}\left[\frac{\mu c^2}{B^2}\right]^{2/3}F . \tag{8}$$

Our earlier assumption of $m=0$ reduces the Hamiltonian further to

$$H=\frac{p_\rho^2}{2}+\frac{p_z^2}{2}+\frac{\rho^2}{2}-\frac{1/2}{(\rho^2+z^2)^{1/2}}+\frac{\lambda z}{8} . \tag{9}$$

Instead of having to solve a new Hamiltonian for every contribution of electric and magnetic fields, we can solve Eq. (9) for one λ and adapt the results to various magnetic field strengths through the B dependence of the units: for instance, the value of $\hbar$ is now magnetic-field dependent. This aspect becomes important in considering the width of the initial wave packet discussed later in this paper. The Coulomb singularity may be removed by working in semiparabolic coordinates [15,34],

$$\rho=u^2-v^2 , \quad z=2uv \quad \text{where } r=(\rho^2+z^2)^{1/2} \tag{10}$$

and changing the time scale by [35]

$$dt/d\tau = 4r \quad \text{("regularization")} . \tag{11}$$

Let $E=H$ be the energy of the electron in the (ρ,z) frame,

$$E=\frac{1}{2}\left\{\left[\frac{d\rho}{dt}\right]^2+\left[\frac{dz}{dt}\right]^2+\rho^2-\frac{1}{r}+\frac{\lambda z}{4}\right\} . \tag{12}$$

E, in the new coordinates, becomes

$$2E=\frac{1}{4r}(p_u^2+p_v^2)+(u^2-v^2)^2-(u^2+v^2)^{-1}+\frac{\lambda}{2}uv , \tag{13}$$

where $p_u=du/d\tau$ and $p_v=dv/d\tau$. The Hamiltonian in the (u,v) frame can be obtained by multiplying by $2r$. This yields the pseudo-Hamiltonian

$$K=2=\tfrac{1}{2}(p_u^2+p_v^2)-4E(u^2+v^2) +2(u^2+v^2)(u^2-v^2)^2+\lambda uv(u^2+v^2) . \tag{14}$$

Thus electron energy becomes a parameter in the pseudo-Hamiltonian which determines the frequency of the two-dimensional isotropic oscillator portion.

III. CORRELATION AND SELECTION OF PARAMETERS

Our method is based on semiclassical computation of the survival probability for the electron. The classical analog of the survival probability is the autocorrelation function for the classical distribution of initial conditions [9,10,27].

We can define the survival probability as the square magnitude of the Fourier transform of the intensity distribution $I(E)$ [9,10]:

$$C_q(t)=\left|\int dE\, e^{-iEt/\hbar} I(E)\right|^2 . \tag{15}$$

This probability can also be expressed as [10]

$$C_q(t)=\mathrm{Tr}\hat{\rho}(0)\hat{\rho}(t) , \tag{16}$$

where

$$\hat{\rho}(0)=|k\rangle\langle k| \tag{17}$$

is the density operator for the initial state $|k\rangle$ and

$$\hat{\rho}(t)=e^{-iHt/\hbar}|k\rangle\langle k|e^{iHt/\hbar} . \tag{18}$$

The classical analog of this quantum correlation function is a density-density autocorrelation function [10,27]:

$$C_c(t)=\int d\mathbf{p}\, d\mathbf{q}\, \rho(\mathbf{p}(0),\mathbf{q}(0))\rho(\mathbf{p}(t),\mathbf{q}(t)) . \tag{19}$$

The initial distribution $\rho(0)$ must be made to correspond with the distribution inherent in the initial wave-packet by a Wigner or Husimi transform [32,36]. We take the initial distribution in the electronic wave packet to be

$$\phi_i(0)=\prod_j \frac{\sqrt{\alpha_j}}{\pi^{1/4}} e^{-\alpha_j^2/2(q_j-q_j^*)^2} e^{iq_jp_j^*/\hbar} , \tag{20}$$

where (p_j^*,q_j^*) is the center of the packet.

The Wigner transform [36] is defined as

$$W(\mathbf{p},\mathbf{q})=h^{-N}\int d\mathbf{x}\, e^{i\mathbf{p}\cdot\mathbf{x}/\hbar}\phi(\mathbf{q}-\mathbf{x}/2)\phi(\mathbf{q}+\mathbf{x}/2) . \tag{21}$$

For our distribution, this definition yields

$$W(\mathbf{p},\mathbf{q})=\rho(\mathbf{p},\mathbf{q}) =h^{-N}\pi^{-N}\prod_j e^{-\alpha_j^2(q_j-q_j^*)^2} e^{-(p_j-p_j^*)^2/\hbar^2\alpha_j^2} . \tag{22}$$

We will calculate $C_c(t)$ by the Monte Carlo method

$$\int dV f(\mathbf{x})=\frac{V}{M}\sum_{i=1}^{M} f(\mathbf{x}_i) , \tag{23}$$

where the points $\mathbf{x}_i$ are uniform randomly distributed over the volume V.

With the uniform distribution of points the $\rho(0)$ term becomes a weighting factor. We have incorporated this weighting in the selection of sample points. We thus use a random Gaussian distribution of initial conditions of width $1/\alpha_j$. The correlation function is now

$$C_c(t)=\frac{1}{M}\sum_k \rho(\mathbf{p}_k,\mathbf{q}_k,t) , \tag{24}$$

where $(\mathbf{p}_k,\mathbf{q}_k)$ is the random Gaussian distribution of initial conditions centered about $(\mathbf{p}^*,\mathbf{q}^*)$.

A set of parameters α_j has been used to set the scale for the distribution of initial conditions, the width of the Gaussian distributions (Fig. 1). We have chosen all of the α_j to be identical and equal to

$$\alpha_j=\sqrt{w/\hbar} , \tag{25}$$

where $w=5$ and $\hbar=0.015$. The set of initial conditions is then obtained by creating a pseudorandom Gaussian distribution for u, v, p_u, and p_v, whose width is unity. The position coordinates are then divided by α_j and the momentum coordinates are multiplied by $\hbar\alpha_j$. These are then added to the u, v, p_u, and p_v values for the center of the packet.

With our initial wave packet, the parameter E is calcu-

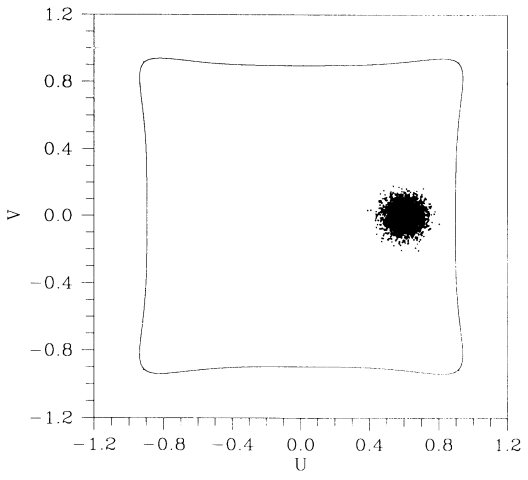

FIG. 1. The location and size, in classical magnetic units (see text), of the simulated wave packet, for $\lambda=0.0$ and $E=-0.3$, within the curve which bounds the motion in the (u,v) frame.

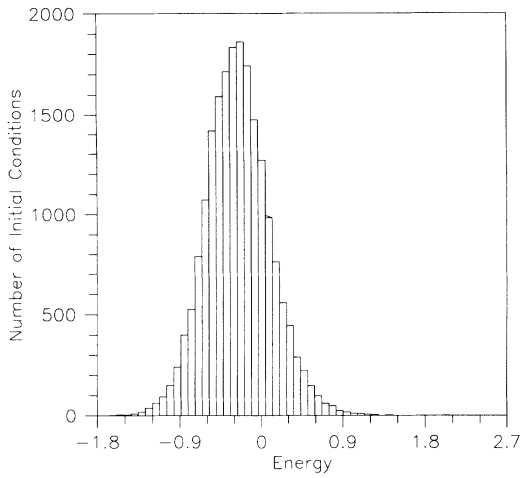

FIG. 2. The energy distribution for a simulated wave packet. This is a Gaussian distribution centered approximately at $E=-0.3$ (in classical magnetic units, see text).

lated to satisfy the Hamiltonian for each point in the packet; see Fig. 2. Each of the initial points is then propagated by means of a fourth-order Runge-Kutta routine. The fixed time steps make the autocorrelation calculation for the packet much simpler. Both the autocorrelation of each trajectory and the contribution of each trajectory to the autocorrelation for the packet are calculated.

IV. RESULTS

We will give a basic analysis of a simulated wave packet started at $u=0.6$, $v=p_v=0.0$, with p_u chosen so that $E=-0.3$ at the center of the packet. Figure 1 shows the initial wave packet and the curve which bounds the motion at $E=-0.3$. We have selected this energy because Harada and Hasegawa [37] found that the chaotic fraction of phase space in QZE begins to increase significantly at $E=-0.35$. At this energy we find that most of our trajectories are chaotic in the SQZE problem. The correlation plots for scaled electric field λ between zero and nine can be found in Fig. 3. The spectra change their appearance noticeably (qualitatively) at $\lambda=2.2$ and 5.6. We determine which classical orbits contribute the most to the correlation, by observing the frequency with which a given periodic orbit appears in the packet. Then plots are made of the most significant contributors for a given field value. An example of this can be found in Fig. 4, for $\lambda=0.0$. For the periodic orbits we use the nomenclature of Wintgen and Friedrich [7], who also shows the appearance of the periodic orbits for zero electric field. Their properties are summarized in Ref. [11], Table I. An alternative naming convention for some periodic orbits appears in Mao and Delos [38].

A. $\lambda=0.0$ (QZE)

At $\lambda=0.0$, the quasi-Landau oscillations in the QZE define the spectrum [see Fig. 3(a)]. These are dominated by the in-line orbit I_1 Fig. 4(a). Yet there is a large variety of orbits which contribute to the correlation. All

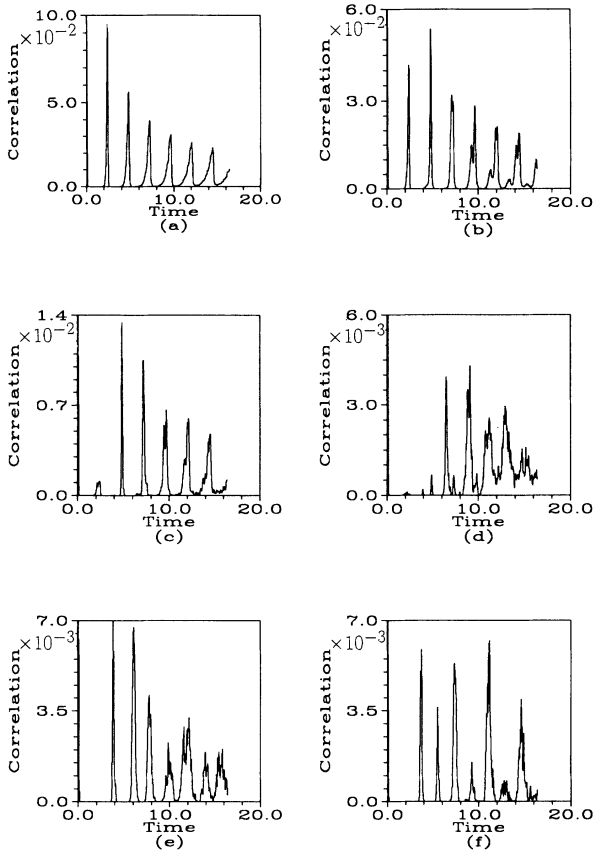

FIG. 3. Autocorrelation plots for the simulated wave packet for constant magnetic field and electric fields (a) $\lambda=0.0$, (b) $\lambda=1.0$, (c) $\lambda=2.2$, (d) $\lambda=3.2$, (e) $\lambda=5.6$, and (f) $\lambda=8.6$. The wave packet was started at $u=0.6$, $v=0.0$, $p_v=0.0$, and p_u (in classical magnetic units, see text) chosen such that $E=-0.3$ at the center of the packet (see Figs. 1 and 2).

of these orbits have a tendency to oscillate horizontally, along the I_1 path. These orbits include III_4 [Fig. 4(b)] and IIb_0 [Fig. 4(c)], as well as many previously unnamed orbits. Some of the orbits approach but do not pass through the origin and therefore are unimportant in the photoionization process. The width of the peaks increases with time. This is due to trajectories which are not perfectly periodic, as well as the appearance of trajectories with very long periods which give very small contributions.

B. $\lambda=1.0$

At $\lambda=1.0$ the electric field starts to distort the spectrum [compare Figs. 3(a) and 3(b)]. The I_1 orbit is now much more weakly represented. The dominant orbit becomes IIb_0 [Fig. 5(a)], as can be seen by the relative height of the second peak, where IIb_0 has its largest effect. We also have significant effects from the III_8 orbit [Fig. 5(b)]. III_8 is responsible for the splitting of the peaks after $t=7.0$. At $\lambda=1.0$ several higher-order orbits appear and these help to account for the increased amount of structure at long times.

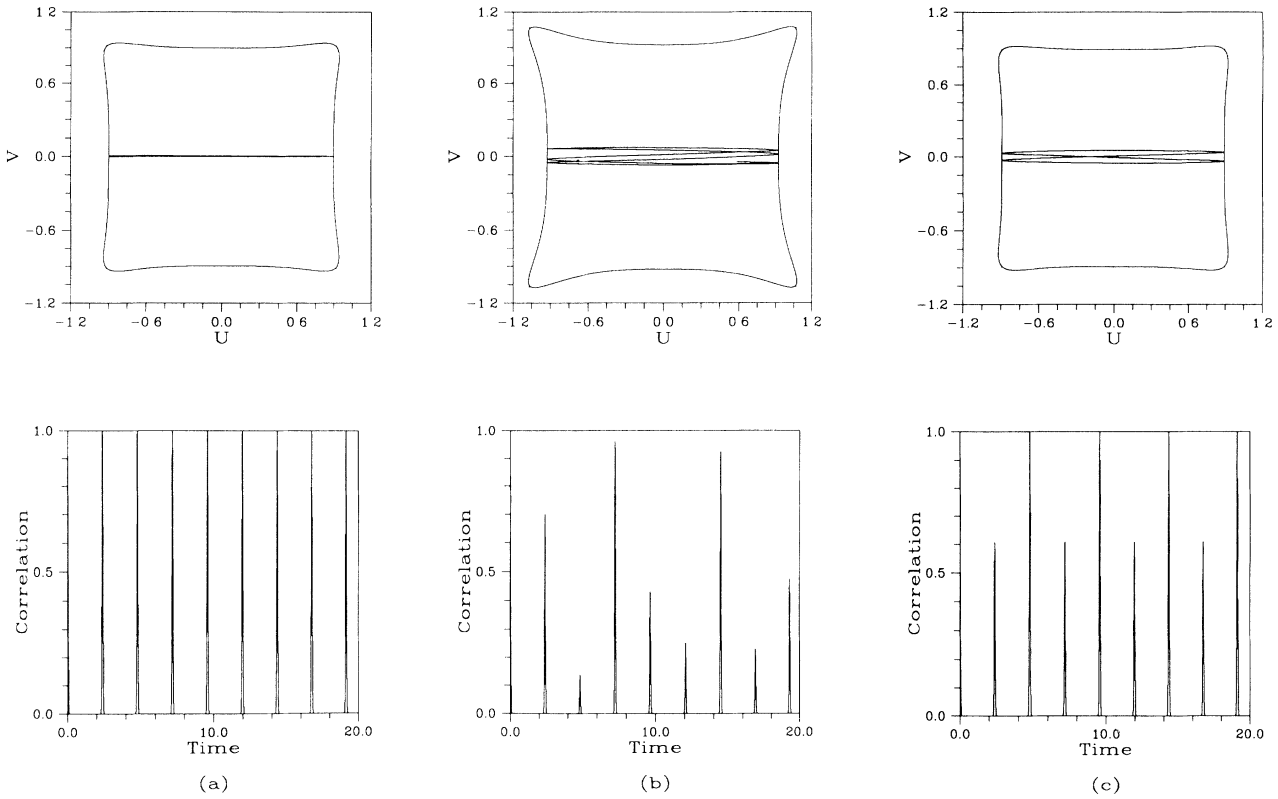

FIG. 4. Plots of important recurring orbits contained within the bounding curve for the motion for $\lambda=0.0$, in classical magnetic units (see text). Below the orbit is a graph of the correlation function for that orbit.

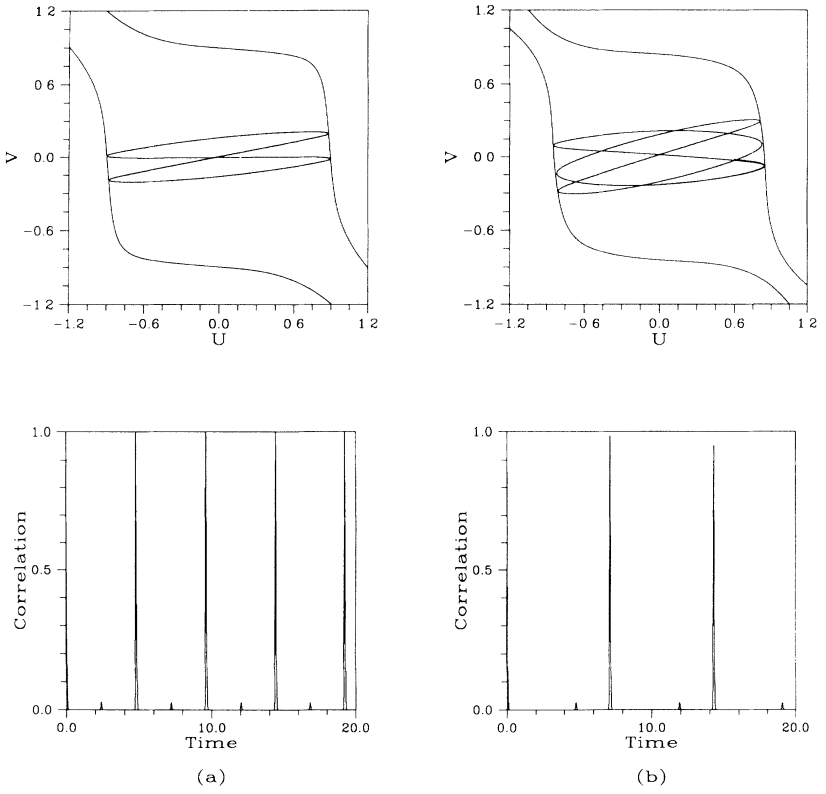

FIG. 5. Plots of important recurring orbits contained within the bounding curve for the motion for $\lambda=1.0$, in classical magnetic units (see text). Below the orbit is a graph of the correlation function for that orbit.

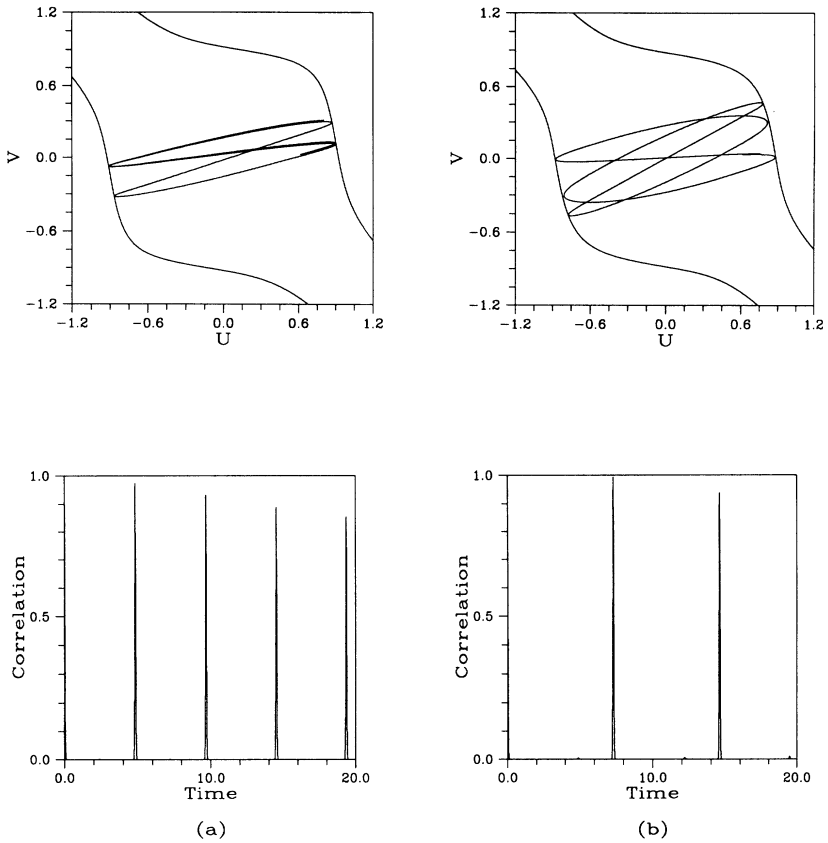

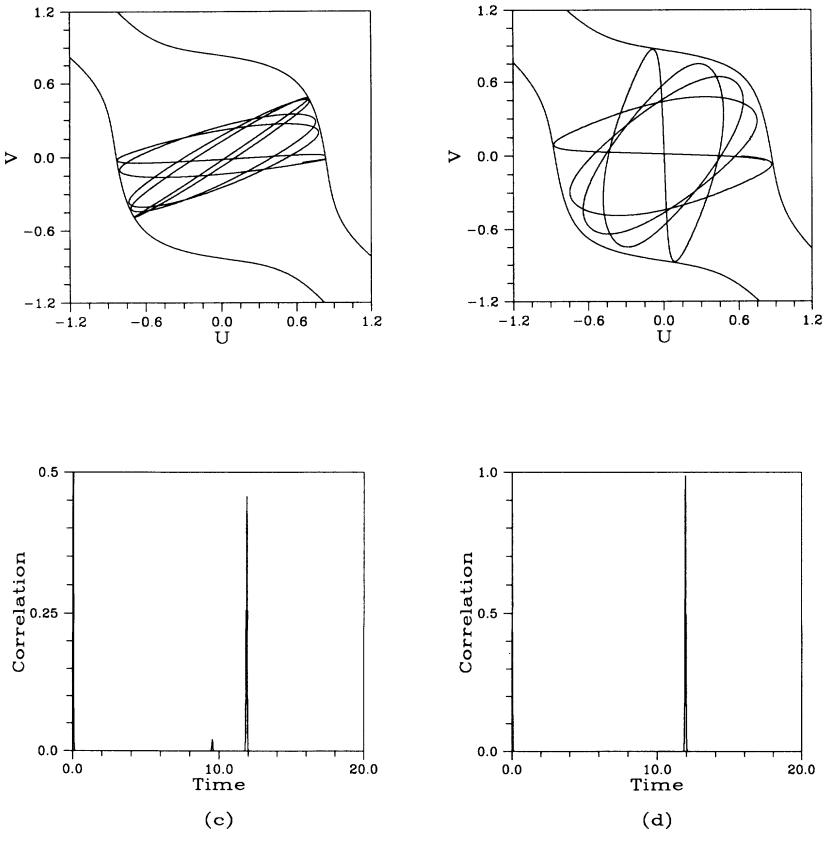

FIG. 6. Plots of important recurring orbits contained within the bounding curve for the motion for $\lambda=2.2$, in classical magnetic units (see text). Below the orbit is a graph of the correlation function for that orbit.

C. $\lambda=2.2$

At $\lambda=2.2$ [Fig. 3(c)] the first peak of $\lambda=1.0$ [Fig. 3(b)] has disappeared. This field strength is large enough to cause considerable ionization and thus only the most stable orbits will contribute. The peak that was previously associated with the I_1 orbit, at $t=2.0$, has now effectively vanished. The IIb_0 orbit [Fig. 6(a)] still gives the strongest contribution. The effect of the IIb_0 orbit is seen in the first and third peaks in the correlation. The III_8 orbit [Fig. 6(b)], also makes a strong appearance at the second and fifth peaks. The fourth peak is dominated by the orbits in Figs. 6(c) and 6(d). At $\lambda=2.2$, Fig. 6(b) and higher-order members of its family all contribute, yet we do not see the lower-order forms of Fig. 6(d) until the electric field increases further. The correlation still exhibits oscillations similar to those seen in the QZE.

As the electric field is increased further, the number of points whose trajectories quickly lead to ionization becomes large around $\lambda=2.5$. This, of course, is expected [see Figs. 7(a) and 7(b)], but does lead us to put one condition on the contributions to the correlation function. We do not consider the contribution to the correlation of trajectories which ionize for relatively short times. The reason for this is twofold. First, the contribution of such trajectories only consists of a spike starting at $t=0.0$, which dies off as the electron propagates from the initial packet. But, they do not return, so the remainder of its contribution is negligible. Second, the inclusion of such orbits simply scales down the autocorrelation for the packets, because of the rescaling by the number of trajectories. This reduction in scale only serves to make analysis of the data more difficult.

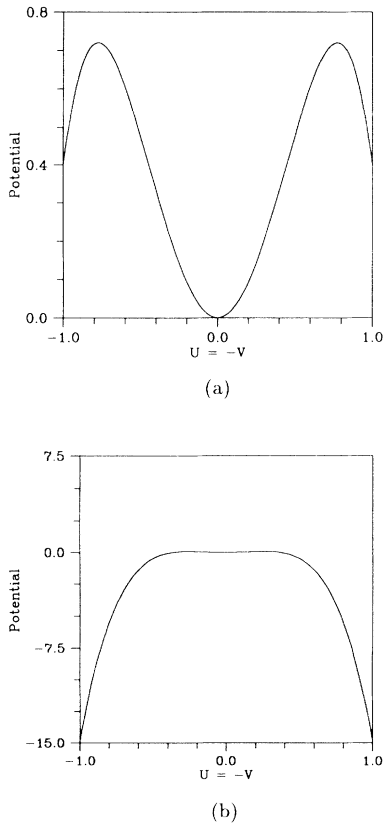

FIG. 7. Potential-energy profiles for (a) $\lambda=1.0$ and (b) $\lambda=8.6$, in classical magnetic units (see text). The figures show cuts through the diagonal $u=-v$. The very shallow well at the top of the $\lambda=8.6$ case can only keep a few stable orbits—most orbits lead to ionization, thus reducing the sample size.

D. $\lambda=3.2$

By $\lambda=3.2$ [Fig. 3(d)] the electric field starts to dominate the system. No hint of the quasi-Landau oscillations is left. The overall magnitude of the correlation is significantly depleted. Only one family of orbits contributes significantly at this field strength; see Figs. 8(a) – 8(c). Each of these related orbits corresponds to different peaks in the correlation. Figure 8(a) gives rise to the peaks at $t=6.5$ and 13.0, while Fig. 8(b) corresponds to the peak at $t=9.0$, and Fig. 8(c) at $t=11.0$.

E. $\lambda=5.6$

At $\lambda=5.6$ [Fig. 3(e)] some structure reappears due to the I_2 orbit [Fig. 9(a)]. The orbit which dominated the $\lambda=3.2$ [Fig. 9(a)] correlation still contributes noticeably; see Fig. 9(b). The peaks at $t=4$, 8, 12, and 16 are due to the I_2 orbit. The peaks at $t=6$ and 12 are caused by the orbit in Fig. 9(b). Now a very small number of points in the wave packet survive for any length of time. This can be seen from the very small correlation values ($\sim 7\times 10^{-3}$). We also no longer see orbits with long periods in the correlation.

F. $\lambda=8.6$

Here [Fig. 3(f)] the I_2 orbit [Fig. 10(a)] becomes more stable than in the previous case, thus giving substantial contributions at later times. The peaks at $t=3.8$, 7.5, 11.0, and 14.4 are mainly due to this orbit. The peak at $t=5.8$ is due to the orbit in Fig. 10(b); this orbit also contributes to the peak at $t=11.0$. The very small peak at $t=9.5$ is from the orbit in Fig. 10(c). We again see an unambiguous periodic structure to the correlation, even though the electric field is very strong.

V. EVOLUTION OF PERIODIC ORBITS, PHASE SPACE, AND SPECTRA

Transitions that occur with changing electric field at constant magnetic field and energy can be viewed in two different ways: One can analyze the evolution of specific periodic orbits for properties such as bifurcations [20,38]. Alternatively, one can focus on a given area in phase space and analyze how various periodic orbits populate that region as conditions are changed. This latter procedure is more appropriate for us because the initial location of our wave packet (which in the Franck-Condon approximation corresponds to the extent of the ground state) determines the subsequent evolution of the spectrum. Changes in the orbits occurring in a fixed region of space (such as at a fixed angle from an axis) arise from the changes in the potential in that region and give informa-

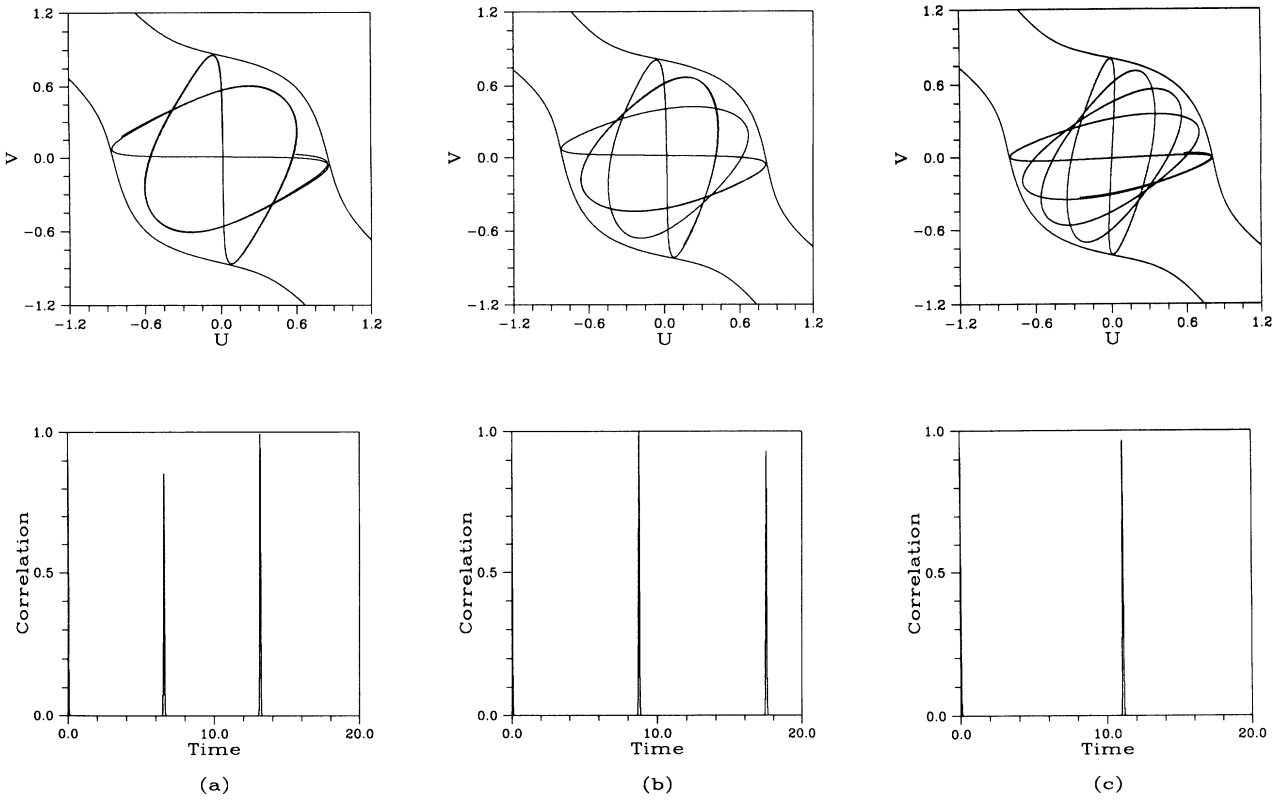

FIG. 8. Plots of important recurring orbits contained within the bounding curve for the motion for $\lambda=3.2$, in classical magnetic units (see text). Below the orbit is a graph of the correlation function for that orbit.

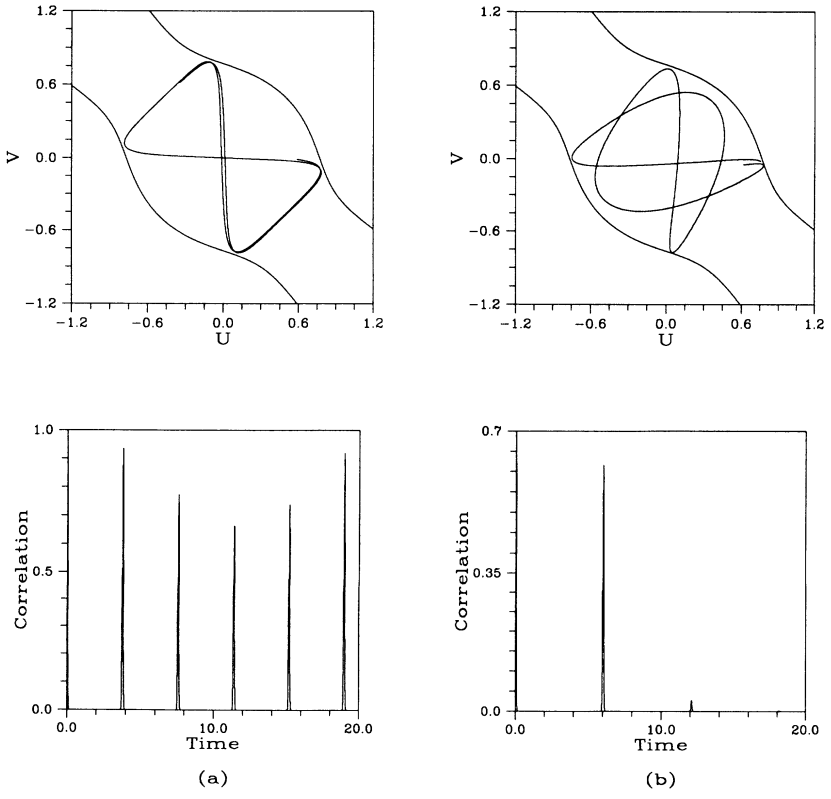

FIG. 9. Plots of important recurring orbits contained within the bounding curve for the motion for $\lambda=5.6$, in classical magnetic units (see text). Below the orbit is a graph of the correlation function for that orbit.

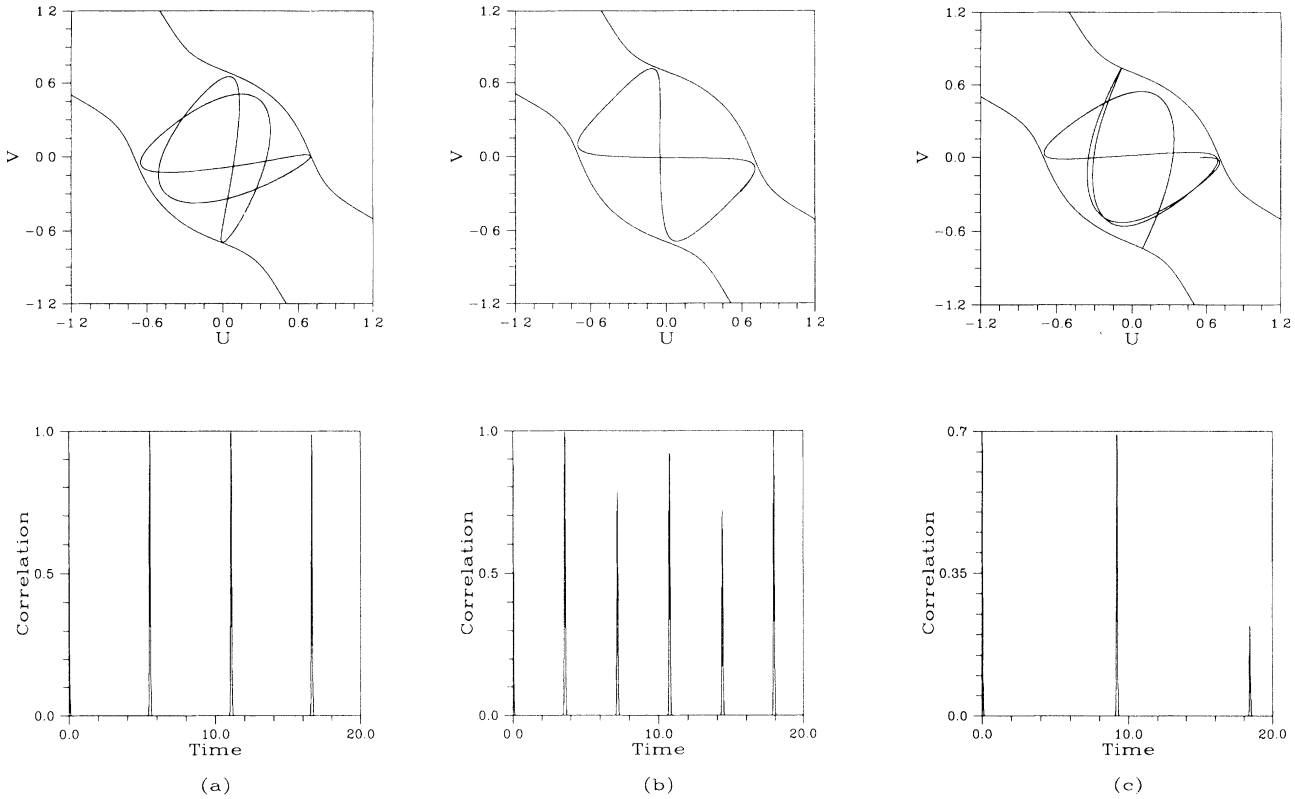

FIG. 10. Plots of important recurring orbits contained within the bounding curve for the motion for $\lambda=8.6$, in classical magnetic units (see text). Below the orbit is a graph of the correlation function for that orbit.

tion on dominant periodic orbits at a given electric-field strength.

For zero electric field, the designation I_2 was given to the orbit in Fig. 11. We will use this orbit as a demonstration. As was mentioned by König *et al.* [20], the electric field breaks the symmetry of the diagonal axes in the (u,v) frame. This creates a significant difference between orbits that follow the trough along the $u=v$ axis and those perpendicular to this axis. It should be noted that both of these axes in the (u,v) frame are parallel to the field, one along the positive axis, the other the negative axis. This transition is concerned with the I_2 orbit about the negative field axis; see Fig. 11(a). As the electric-field parameter λ is increased from zero to seven, the orbits in the (u,v) frame simply compress along the field without significant changes in shape. However, in the (ρ,z) frame the shape of the orbit changes dramatically, see Fig. 11(b). The starting angle for the stable trajectories changes from 59° at zero field to 106° at $\lambda=7.0$. The final shape is identical to the IIb_0 orbit, except it is rotated by 90°.

When we start a wave packet at a particular location with a specific momentum, we determine the behavior of the spectra. Orbits which recur in this region will be the important contributors to the spectrum because the majority of the points in the wave packet will move through this region at approximately the same momentum as the packet's center. By searching a small region of the (u,v) plane for periodic orbits at a given electric field, we can predict which orbits will be most important at various field strengths. The plots in Fig. 12 are for the case shown in Fig. 1 (with $u_0=v_0=p_v=0$ initially). We know that the zero-electric-field spectra have a large contribution from the I_1 orbit, which is the orbit obtained with these initial conditions for the $\lambda=0$ case. By analyzing which orbits are obtained for these same initial conditions as λ is increased, we can anticipate which orbits will dominate this spectrum at higher electric-field strengths without having to actually calculate the entire spectrum for each field strength.

As the electric field is increased, the shape of the potential changes dramatically [see Figs. 7(a) and 7(b)] and different classical orbits become dominant at various field strengths and at different initial positions for the packet. In Fig. 3, we display the correlation plots for $E=-0.3$, $v=p_v=0.0$, and $u=0.6$ (i.e., for a wave packet that starts out on the u axis; see Fig. 1). This region, with the periodic orbits it contains, will tend to dominate the spectra as the electric field is increased. At $\lambda=0.0$ the spectrum contains contributions from the I_1, IIb_0, and III_4 orbits (see Sec. IV A). In this case, the most prominent orbit I_1, as would be expected on the basis of its geometry, i.e., because it is along the u axis. We can then compare the correlation plots to the transition of the $\theta=0.0°$ region (Fig. 12). These plots indicate that the dominant orbit in the $\lambda=1.0$ case will be the IIb_0 orbit. In the correlation plot for $\lambda=1.0$ [Fig. 3(b)], we see that peak 1 has shrunk significantly, but peak 2 is approximately the same size. We no longer see the I_1 orbit at peak 1; instead we see a large number of orbits which follow along

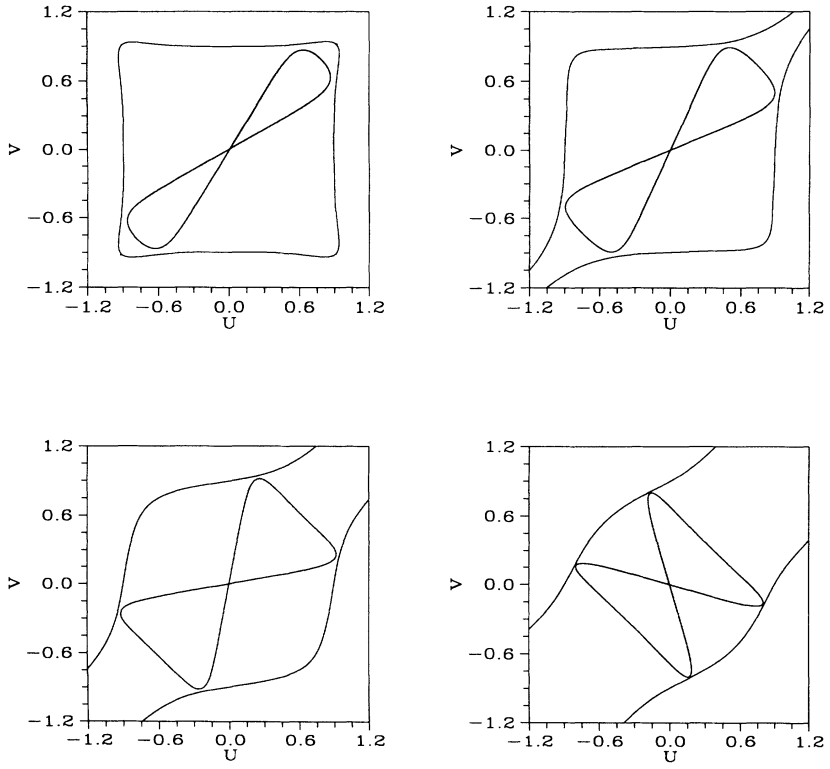

(a)

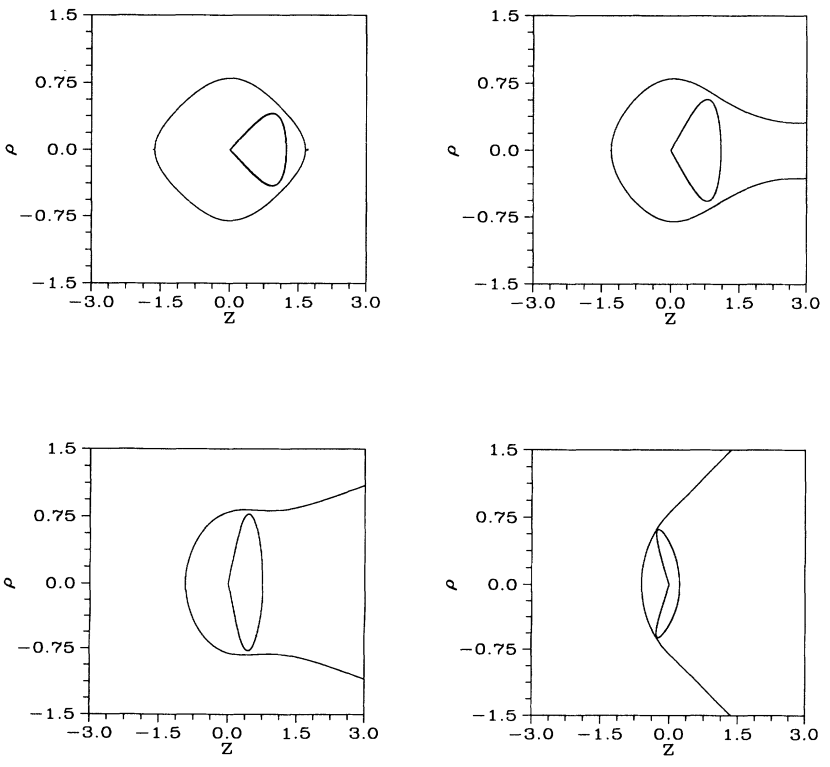

(b)

FIG. 11. The evolution of the I_2 orbit with increasing electric field at $E=-0.3$. The values of λ are $\lambda=-0.1$, -0.5, -2.0, -7.0. Both the (a) (u,v) and (b) (ρ,z) plots, in classical magnetic units (see text), are shown.

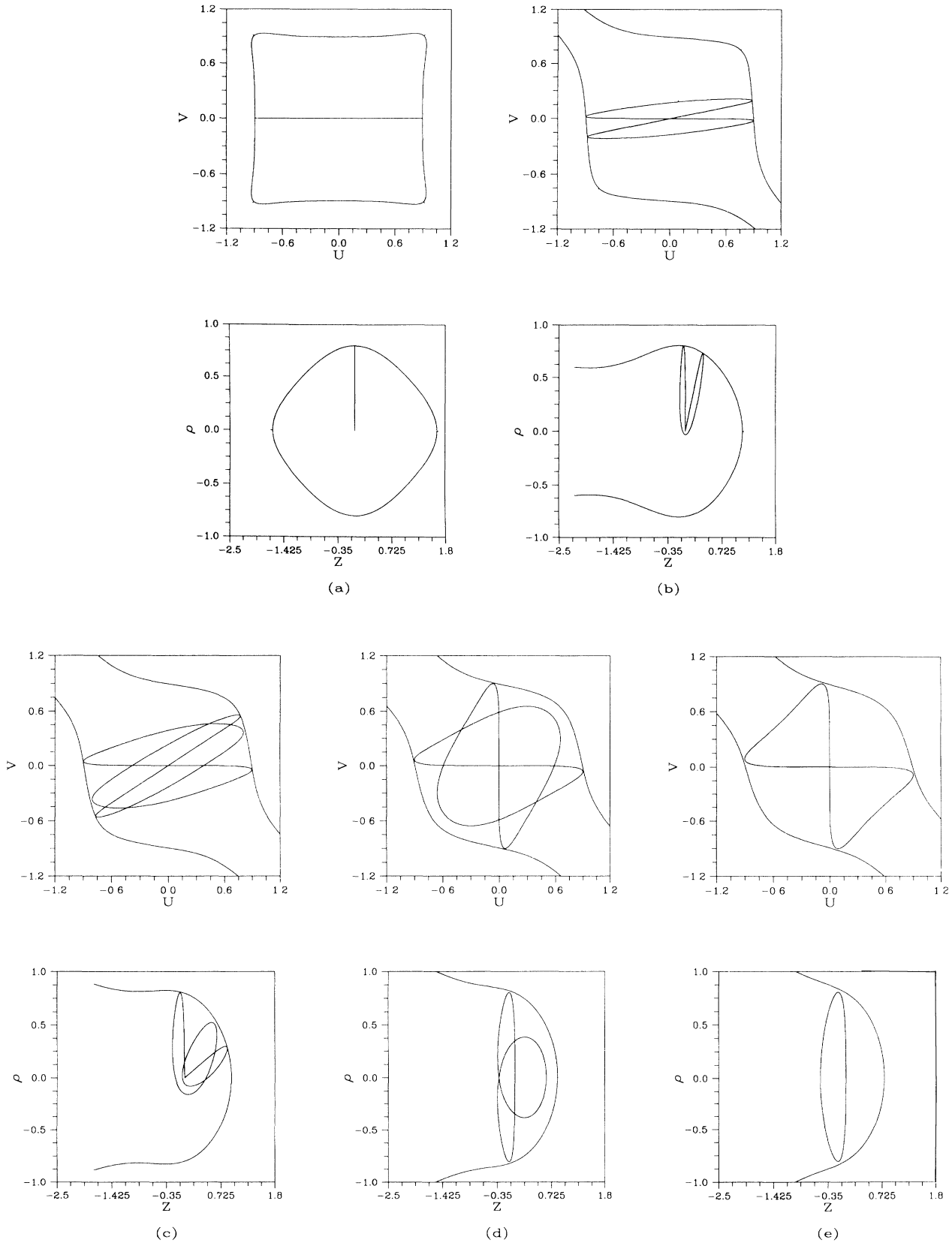

FIG. 12. Dominant periodic orbits for a variety of electric fields λ: (a) $\lambda=0.0$, (b) $\lambda=0.96$, (c) $\lambda=2.0$, (d) $\lambda=2.74$, and (e) $\lambda=3.62$, started at the origin and initially moving along the u axis. Both the (u,v) and the (ρ,z) plots, in classical magnetic units (see text), are shown.

the direction of the axes, such as Fig. 5(a) (IIb_0) and Fig. 5(b) (III_4). Peak 2 is strongly dominated by the IIb_0 orbit, with additional contributions by some higher-order orbits.

At $\lambda=2.0$, Fig. 12(c) predicts the dominance of the III_8 orbit. The correlation plot for $\lambda=2.2$ [Fig. 3(c)] shows the disappearance of the peak at $t=2.0$. Peak 1 is due to the IIb_0 orbit, but these orbits are now much less stable. Peak 2 is due to the III_8 orbit. Peak 3 has contributions from the IIb_0 orbit. The Fig. 6(c) orbit appears at peak 4 with another ten-lobed orbit with identical structure, but symmetric with respect to the field [see Fig. 6(d)]. Peak 1 for $\lambda=3.2$ [Fig. 3(d)] is dominated by the orbit in Fig. 8(a). This orbit also appears as the dominant one in the region along $\theta=0$ when the electric field is $\lambda=2.74$; see Fig. 12(d). Figures 8(b) and 8(c) orbits constitute peaks 2 and 3, respectively.

We see from Fig. 9(a) that the I_2 orbit determines peak 1 for the $\lambda=5.6$ correlation. Peak 2 is due to the orbit in Fig. 9(b). Peak 3 is also due to the I_2 orbit. From examining dominant periodic orbits in the $\theta=0$ region, we found that I_2 is prominent only when $\lambda\cong 3.6$.

The apparent contradiction between this observation and the prominence of the I_2 at $\lambda=5.6$ [evident by Fig. 9(a)] can be explained by realizing that in our wave-packet calculation the energies for the points in the packet are all different. In fact, they form a Gaussian distribution in the energy (see Fig. 2). Orbits with higher energy are more prominent in the spectrum. This becomes more dramatic as the electric-field strength increases. To accurately predict the spectra for various λ, we must change the energy at which we propagate the $\theta=0°$ trajectory. For the I_2 orbit, the energy of surviving trajectories is $\cong -0.63$. When we focus on this energy, we find I_2 at $\lambda=5.7$ (see Fig. 13), which is where we get the largest contribution from I_2 according to Fig. 9(a).

Of course, this approximate calculation does not simulate all of the structure of the spectra. However, it does allow us to see quickly which orbits will contribute at any electric field. Many orbits will be found, and these will give a good indication of how the system is evolving.

Calculating wave-packet correlations yield many recurring orbits in addition to those that pass identically through the origin. Some of these orbits are shown in Fig. 14.

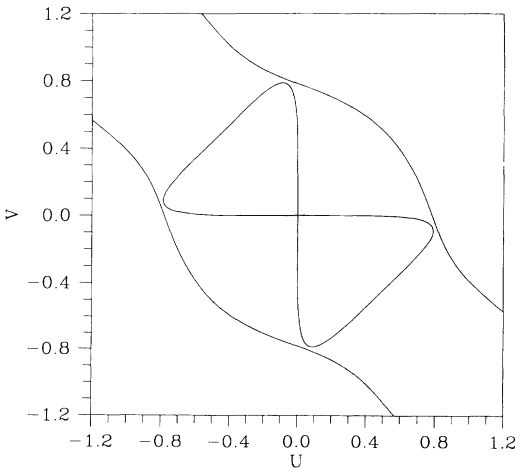

FIG. 13. The I_2 orbit at $\lambda=5.72$ and $E=-0.63$, in classical magnetic units (see text).

VI. DISCUSSION

In this paper, electronic spectra, the most quantal of all phenomena, are simulated classically. Not only that, but the inherent advantages of classical mechanics are exploited to the maximum to tell us which of the infinity of periodic orbits contribute and to which parts of the spectrum. The fundamental reasons for performing many of the state-of-the-art experiments on Rydberg states is to address the issue of the relationship between classical and quantum mechanics, i.e., the correspondence principle. Many experimentalists would ideally like to perform experiments on the hydrogen atom but often cannot for technical reasons. Nevertheless, the hydrogen atom is the prototypical Rydberg atom and is, fortunately, easier to deal with computationally than say Ba. The important experiments of König *et al.* [20] on Ba reveal many interesting features but are difficult to simulate in detail because of the non-pure-hydrogenic nature of the Ba Rydberg states and *experimental uncertainties as to the precise nature of the initial state.* While our simulation approximates the experimental conditions only roughly, a comparison of the results with those of König *et al.* [20] shows qualitative agreement on a variety of points, including the approximate locations at which the appearance of the spectrum changes and the sequence in which periodic orbits appear and disappear in the spectra. For instance, the periodic orbit IIb_0 is the first one to appear (in addition to the quasi-Landau oscillations I_1) when a small electric field is added to the magnetic field. Also, as the electric field is increased, the spectra are increasingly dominated by I_2. For very large electric fields, periodic orbits along the electric field direction [26] (denoted as z_i by König *et al.* [20]) mix with the orbits familiar from the magnetic field case. The disagreements that we see are that in our large electric-field cases, first we do not see many harmonics of the same periodic-orbit contributing and second the orbit IIb_1 has never appeared in our spectra. In conclusion, we summarize the main points revealed by our study.

(i) The hydrogen-atom system in parallel electric and magnetic fields is of great theoretical and potential experimental importance. The classical mechanical simulations were performed on a fixed pseudoenergy manifold for which the actual energy occurred as a parameter. This stands in marked contrast to previous calculations where the Hamiltonian and the physical energy are the same. Extraction of the autocorrelation function in coordinates constructed to remove the Coulomb singularity is delicate, but represents a *practical* route to the computation of electron survival probabilities semiclassically, as we demonstrated and stress again here that this is an approach free of troublesome numerical problems associated with the Coulomb term in the potential energy.

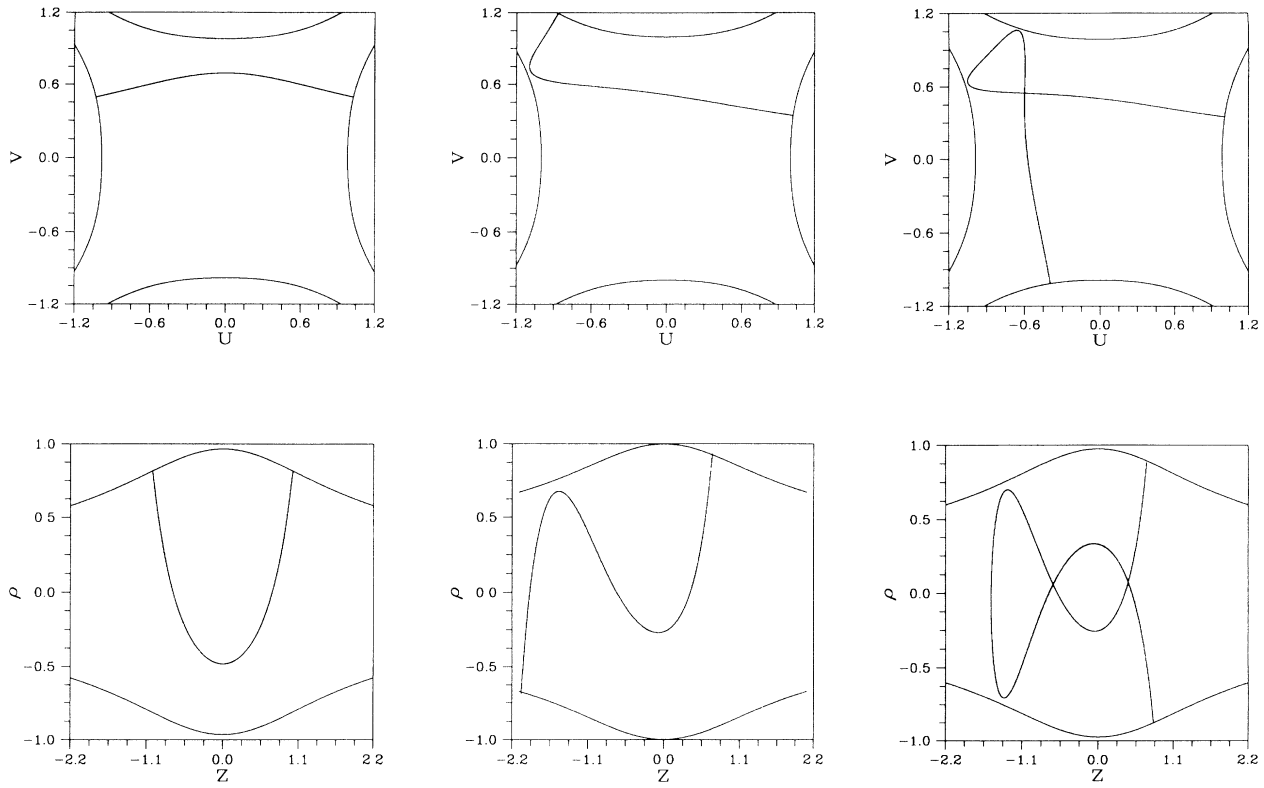

FIG. 14. Some of the orbits which do not pass through the origin. These were all found by propagating simulated wave packets.

(ii) The transition from the QZE to the Stark regime was mapped out and the associated changes in the spectra computed and related to particular periodic or recurring orbits. This established the classical origins of various spectral features. One wants to separate what are essentially classical effects from other details. Thus the coincidence between the general observation of König *et al.* for Ba and the theoretical results for H point to the robustness of correspondence principle arguments and classical simulations of electronic spectra. This should serve to stimulate experiments for H and future calculations on the Ba atom. The striking relationship between spectral features and periodic orbits only adds to the growing evidence and database that suggests that classical simulations of electronic spectra will be eminently useful even when it is difficult to find periodic orbits explicitly. We also note that extraction of periodic orbits cannot be done using some "black box" algorithm but relies partly on computational experiments. Our approach is unique in that in constructing the correlation function for the ensemble we also carried along the correlation for the individual members of the ensemble of trajectories. This allowed us to identify and pick out the individual trajectories that are dominant.

(iii) The parallel-electric- and magnetic-field problem allows one to monitor spectral changes as one goes from one symmetry limit to another and thus provides an important test of the classical simulation of electronic spectra for chaotic multidimensional problems. Thus we find that spectra are often dominated by periodic orbits *even when the system contains nontrivial symmetries.* Therefore, classical simulations may be extremely useful when one cannot or does not care to find periodic orbits. Such is the case in more than two degrees of freedom where the classical approach developed here will present a basis for future work. Such work is currently in progress.

Note added. The oscillations in the absorption spectrum of barium in parallel fields has recently been analyzed in terms of periodic orbits by Mao *et al.* [40]. A method different from that used in our work has also proven powerful in locating stable periodic orbits in chaotic systems [41].

ACKNOWLEDGMENTS

We are grateful to Professor H. S. Taylor for enlightening discussions. We thank David Farrelly for editorial comments on an earlier version and Dr. Herbert Smew for an insightful comment. This research was supported by the National Science Foundation and by DGYCIT (Spain) under Project No. PB89-117. We gratefully acknowledge support from MEC (Spain) under programs Movilidad de Personal Investigador (F. B.) and Proyectos de Investigacion Internacionales al Amparo de Convenios Interuniversitarios (R. M. B. and T. U.).

[1] J. C. Gay and D. Delande, in *Atomic Excitation and Recombination in External Fields,* edited by M. H. Nayfeh and C. W. Clark (Gordon and Breach, New York, 1985), p. 131.
[2] For example, T. F. Gallagher, Rep. Prog. Phys. **51**, 143 (1988).
[3] H. Friedrich and D. Wintgen, Phys. Rep. **183**, 37 (1989).
[4] For reviews, see H. Hasegawa, M. Robnik, and G. Wunner, Prog. Theor. Phys. Suppl. **98**, 198 (1989).
[5] D. Delande and J. C. Gay, Comments At. Mol. Phys. **19**, 35 (1986).
[6] D. Delande, in *Chaos and Quantum Physics,* 1989 Les Houches Lectures Session LII, edited by M.-J. Giannoni, A. Voros, and J. Zinn-Justin (North-Holland, Amsterdam, 1991), p. 665.
[7] D. Wintgen and H. Friedrich, Phys. Rev. A **36**, 131 (1987).
[8] M. C. Gutzwiller, *Chaos in Classical and Quantum Mechanics* (Springer-Verlag, New York, 1990).
[9] E. J. Heller, Chem. Phys. Lett. **34**, 321 (1975); J. Chem. Phys. **62**, 1544 (1975); **64**, 63 (1976); **65**, 4979 (1976); **66**, 5777 (1977); **75**, 2923 (1981); Acc. Chem. Res. **14**, 368 (1981).
[10] E. J. Heller, in *Chaos and Quantum Physics* (Ref. [6]), p. 547.
[11] W. P. Reinhardt, J. Phys. B **16**, L635 (1983).
[12] W. P. Reinhardt, in *Atomic Excitation and Recombination in External Fields* (Ref. [1]), p. 85.
[13] W. P. Reinhardt, and D. R. Kerner, in *Proceedings of the XVIth International Conference on the Physics of Electronic and Atomic Collisions, New York, 1989,* AIP Conf. Proc. No. 205, edited by A. Dalgarno, R. S. Freund, M. S. Lubell, and T. B. Lucatorto (AIP, New York, 1990), p. 458.
[14] For recent reviews, see G. Alber and P. Zoller, Phys. Rep. **199**, 231 (1991); G. Alber, Comments At. Mol. Phys. **26**, 47 (1991).
[15] A. R. Edmonds and R. A. Pullen, Imperial College Reports No. ICTP/79-80/28 and No. ICTP/79-80/29, 1980 (unpublished).
[16] R. L. Waterland, J. B. Delos, and M. L. Du, Phys. Rev. A **35**, 5064 (1987); J. B. Delos, R. L. Waterland, and M. L. Du, *ibid.* **37**, 1185 (1988).
[17] T. P. Grozdanov and M. J. Rakovic, J. Phys. B **23**, 3531 (1990); P. A. Braun, *ibid.* **24**, 399 (1991).
[18] E. Korevaar and M. G. Littman, in *Chaos and Quantum Physics* (Ref. [6]), p. 157; F. Penent, D. Delande, F. Biraben, and J. C. Gay, Opt. Commun. **49**, 184 (1984); F. Penent, D. Delande, and J. C. Gay, Phys. Rev. A **37**, 4707 (1988); J. C. Gay and D. Delande, *ibid.* **37**, 131 (1988); P. A. Braun and E. A. Solov'ev, Zh. Eksp. Teor. Fiz. **85**, 109 (1983) [Sov. Phys. JETP **58**, 63 (1984)]; **86**, 68 (1984) [**59**, 38 (1984)].
[19] P. Cacciani, E. Luc-Koenig, J. Pinard, C. Thomas, and S. Liberman, Phys. Rev. Lett. **56**, 1467 (1986); P. Cacciani, S. Liberman, E. Luc-Koenig, J. Pinard, and C. Thomas, J. Phys. B **21**, 3473 (1988); **21**, 3499 (1988); **21**, 3523 (1988); P. Cacciani, S. Liberman, E. Luc-Koenig, J. Pinard, and C. Thomas, Phys. Rev. A **40**, 3026 (1989).
[20] A. König, J. Neukammer, K. Vietzke, M. Kohl, H.-J. Grabka, H. Hieronymus, and H. Rinnerberg, Phys. Rev. A **38**, 547 (1988).
[21] G. Wiebusch, J. Main, K. Kruger, H. Rottke, A. Holle, and K. H. Welge, Phys. Rev. Lett. **62**, 2821 (1989).
[22] G. Raithel, M. Fauth, and H. Walther, Phys. Rev. A **44**, 1898 (1992).
[23] D. Delande and J. C. Gay, Phys. Rev. Lett. **66**, 3237 (1991).
[24] D. Farrelly, T. Uzer, P. E. Raines, J. P. Skelton, and J. A. Milligan, Phys. Rev. A **45**, 4738 (1992), and references therein.
[25] H. Rinneberg, J. Neukammer, A. König, K. Vietzke, H. Hieronymous, M. Kohl, and G. Jönsson, in *Oji International Seminar on Highly Excited States of Atoms and Molecules,* edited by S. S. Kano and M. Matsuzawa (Fuji-Yoshida, Tokyo, Japan, 1986), p. 7.
[26] R. R. Freeman, N. P. Economou, G. C. Bjorklund, and K. T. Lu, Phys. Rev. Lett. **41**, 1463 (1978).
[27] J. M. Gomez-Llorente, S. C. Farantos, O. Han, and H. S. Taylor, J. Opt. Soc. Am. B **7**, 1851 (1990); J. M. Gomez-Llorente and H. S. Taylor, J. Chem. Phys. **91**, 953 (1989).
[28] J. M. Gomez-Llorente, H. S. Taylor, and E. Pollak, Phys. Rev. Lett. **62**, 2096 (1989); J. M. Gomez-Llorente, J. Zakrzewski, H. S. Taylor, and K. C. Kulander, J. Chem. Phys. **90**, 1505 (1989); H. S. Taylor and J. Zakrzewski, Phys. Rev. A **38**, 3732 (1988); J. M. Gomez-Llorente, J. Zakrzewski, H. S. Taylor, and K. C. Kulander, J. Chem. Phys. **89**, 5959 (1989).
[29] S. C. Farantos, J. M. Gomez-Llorente, O. Hahn, and H. S. Taylor, J. Chem. Phys. **93**, 76 (1990); O. Hahn, J. M. Gomez-Llorente, and H. S. Taylor, *ibid.* **94**, 2608 (1991); S. C. Farantos and H. S. Taylor, *ibid.* **94**, 4887 (1991); O. Hahn and H. S. Taylor, *ibid.* **96**, 5915 (1992).
[30] B. Eckhardt, J. M. Gomez-Llorente, and E. Pollak, Phys. Rev. A **39**, 3776 (1989); Chem. Phys. Lett. **174**, 325 (1990).
[31] J. M. Gomez-Llorente, F. Borondo, N. Berenguer, and R. M. Benito, Chem. Phys. Lett. **192**, 430 (1992).
[32] F. Borondo, in *Structure, Interactions and Reactivity,* edited by S. Fraga (Elsevier, Amsterdam, 1992), p. 592.
[33] F. Borondo, J. M. Gomez-Llorente, and R. M. Benito, Laser Chem. **12**, 85 (1992).
[34] A. R. Edmonds, J. Phys. A **22**, L673 (1989).
[35] For example, E. L. Stiefel and G. Scheifele, *Linear and Regular Celestial Mechanics* (Springer-Verlag, Berlin, 1971).
[36] For example, M. V. Berry, Proc. R. Soc. London Ser. A **287**, 237 (1977).
[37] A. Harada and H. Hasegawa, J. Phys. A **16**, L259 (1983).
[38] J.-M. Mao and J. B. Delos, Phys. Rev. A **45**, 1746 (1992).
[39] S. Bivona, W. Schweizer, P. F. O'Mahony, and K. T. Taylor, J. Phys. B **21**, L617 (1988).
[40] J.-M. Mao, K. A. Rapelje, S. J. Blodgett-Ford, and J. B. Delos, Phys. Rev. A **48**, 2117 (1993).
[41] D. Grobgeld, E. Pollak, and J. Zakrzewski, Physica D **56**, 368 (1992).